Nanoscale

RSC Publishing

PAPER

View Article Online
View Journal | View Issue

Cite this: *Nanoscale*, 2013, **5**, 3681

Coarse-grained molecular dynamics simulations of photoswitchable assembly and disassembly†

Xiaoyan Zheng, Dong Wang* and Zhigang Shuai*

Received 13th November 2012
Accepted 20th February 2013

DOI: 10.1039/c3nr33619k

www.rsc.org/nanoscale

The supramolecular self-assembly and disassembly that are responsive to external stimuli are of critical importance to the design and synthesis of functional supramolecular materials. In this work, we performed a coarse-grained molecular dynamics study of photo-controlled assembly and disassembly on a timescale of ten microseconds. The spontaneous assembly of *cis*-AzoC10, *trans*-AzoC10, and *cis*-AzoC10/α-CD into micelle-like aggregates, and the disassembly of *trans*-AzoC10/α-CD starting from a pre-assembled micelle were directly simulated. Our results of simulations have revealed a significant size and shape dependence of aggregates on the molecular structure and concentrations of monomers. As demonstrated, with careful design, coarse-grained molecular dynamics simulations are useful in the study of controlled assembly and disassembly to bridge the gap between atomistic simulations and experiments.

1 Introduction

The assembly and disassembly that are responsive to external stimuli such as pH, temperature, light, and redox state are of central importance in the design and synthesis of functional supramolecular materials that many researchers have been focusing on.[1–6] The azobenzene moiety, a well-studied photo-active system, can undergo *cis–trans* photoisomerization in response to UV and visible light, which can result in the size and polarity change of the azobenzene unit.[7–12] As a result, azobenzene has been widely used in synthetic photo-responsive macromolecules to modulate the structure and functions of nanomechanical devices.[13–15] In particular, *trans*-azobenzene can form an inclusion complex with α-cyclodextrin (α-CD) driven by hydrophobic interactions, but *cis*-azobenzene cannot form an inclusion complex with α-CD due to the size mismatch.[3,4] The light-driven reversible host–guest inclusion and exclusion between azobenzene and α-CD have been utilized to design molecular machines.[16–18] As an example, a photo-controlled reversible assembly and disassembly has been observed in aqueous solution taking advantage of the host–guest interaction between an azobenzene-containing amphiphile 1-[10-(4-phenylazophenoxy)decyl]pyridinium bromide (AzoC10) and α-CD.[4] It was observed that firstly AzoC10 as a surfactant can form vesicles in aqueous solution. Secondly, when α-CD was added, the vesicles disassembled. Thirdly, when the above system was irradiated by UV light, the vesicles were formed again, moreover, the vesicle-like aggregates disassembled by further irradiation of visible light. This reversible assembly and disassembly can be cycled many times. The size and shape of the vesicle-like aggregates formed by *trans*-AzoC10 and *cis*-AzoC10 were similar, but different from those formed by AzoC10 in the presence of α-CD and irradiated by UV light. It indicated that the latter was built from the inclusion complex formed between *cis*-AzoC10 and α-CD.

To understand the molecular basis of the observed photo-switchable assembly and disassembly, we performed atomistic molecular dynamics (MD) simulations of the host–guest inclusion between AzoC10 and α-CD.[19] Our results of simulations showed that both *cis*- and *trans*-AzoC10 can form an inclusion complex with α-CD. For *trans*-AzoC10, the azobenzene moiety is axially included at the central cavity of α-CD. For *cis*-AzoC10, a favorable binding mode is that one of the phenyl rings is exposed to water, while the other is included in the cavity of α-CD. It is also observed that α-CD can shuttle over the long alkyl chain of *cis*-AzoC10. These findings have helped us to understand the experimental observations; *cis*-AzoC10/α-CD was amphiphilic so it assembled, while *trans*-AzoC10/α-CD was not amphiphilic so it disassembled. Based on the atomistic simulations, in this work we investigate the extended assembly of a vast number of host and guest molecules, addressing the size and shape dependence of assemblies on the molecular structure and concentrations of monomers in the photo-controlled assembly. In this case, an all-atom (AA) representation of molecular systems is usually not practical, and the development of coarse-grained (CG) models, in which several heavy atoms are grouped together and represented by one particle, becomes necessary.

MOE Key Laboratory of Organic Optoelectronics and Molecular Engineering, Department of Chemistry, Tsinghua University, 100084 Beijing, People's Republic of China. E-mail: dong913@tsinghua.edu.cn; zgshuai@tsinghua.edu.cn

† Electronic supplementary information (ESI) available: Simulation details with both AA and CG models, and CG force field files for *cis*-, *trans*-AzoC10 and α-CD. See DOI: 10.1039/c3nr33619k

Large-scale molecular dynamics simulations of self-assembling systems using CG models have been at the frontier of theoretical chemistry.[20,21] The assembly of amphiphiles such as surfactants, block co-polymers, and lipids not only represents one of the most intensively investigated systems, but also the most successful ones studied to date using CG molecular dynamics simulations.[22–24] There are currently three major approaches of coarse-graining: (1) reverse Monte Carlo methods,[25–29] (2) force matching schemes,[30–35] and (3) the development of empirical CG force fields.[36–38] The last one is an extension of Smit's approach,[39] where the parameterization of each CG segment was done empirically using selected functional forms. The MARTINI force field,[36,37] which was parameterized to reproduce the partitioning free energies between polar and apolar phases of a large number of chemical compounds, is one of the most successful examples of the CG force fields, particularly in applications to the study of self-assembly in aqueous solution. Recently, CG models for carbohydrates were also developed in the MARTINI force field.[40] This extended model used a mapping of three interaction sites per glucose residue. In this work, we adopted the MARTINI CG scheme to model water molecules as the solvent, AzoC10 the surfactant, and α-CD the cyclic oligosaccharide. It is emphasized that there are existing studies in the literature focusing on the size and shape dependence of aggregates on the molecular structure of monomers, such as short and long chain cationic surfactants[41] and multiheaded surfactants,[42] and there are also reports on the shape dependence of micelles on the surfactant concentrations,[43] but we have not seen any study aiming at addressing this issue in the photo-controlled assembly involving photoisomerization and the host–guest interaction. In this case, sufficient structural features have to be retained in the CG model to distinguish *cis*- and *trans*-isomers of AzoC10, and to characterize the hydrophobic cavity and hydrophilic exterior of α-CD, making our CG simulations much more challenging. Our CG models based on the MARTINI force field were further validated by comparing with the corresponding atomistic models and have been found to be able to capture the amphiphilicity change caused by the host–guest interaction and photoisomerization. Importantly, our ten microsecond molecular dynamics simulations have revealed the size and shape dependence of aggregates on the molecular structure of monomers.

2 Model and simulation methods

2.1 Simulation setup

Table 1 provides a summary of the detailed simulation setup used in this work. Firstly, in order to validate the CG model, we carried out contrast simulations of *cis*-, *trans*-AzoC10, and α-CD with both AA and CG molecular dynamics in a cubic box with dimensions of $15 \times 15 \times 15$ nm, labeled as 1–6 in Table 1. The starting configurations of *cis*- and *trans*-AzoC10 in both AA and CG simulations were a pre-assembled spherical micelle generated by the PACKMOL program;[44] simulations of α-CDs were started from a random distribution in aqueous solution. Secondly, we performed large-scale CG simulations for both *cis*- and *trans*-AzoC10 at four concentrations by randomly placing 500, 1000, 1500, and 2000 surfactants in a cubic box of 30 nm on each side, labeled as 7–14 in Table 1. Lastly, we performed CG molecular dynamics simulations of *cis*-AzoC10/α-CD and *trans*-AzoC10/α-CD complexes in aqueous solution with the cubic box of 30 nm and 15 nm on each side, respectively, labeled as 15–18 in Table 1. The starting configuration of *cis*-AzoC10/α-CD was an ordered arrangement of the inclusion complexes produced in the VMD program.[45] The simulation of *trans*-AzoC10/α-CD was started from a pre-assembled micelle generated with the PACKMOL program.[44]

Table 1 Summary of simulations conducted

Labels	Systems	N_{surf}	N_{water}[a]	L (nm)	Time[b] (μs)
1	*cis*-AzoC10 (AA)	70	107 781	15.0	0.01
2	*cis*-AzoC10 (CG)	70	107 780	14.9	0.1
3	*trans*-AzoC10 (AA)	50	108 356	15.0	0.01
4	*trans*-AzoC10 (CG)	50	108 356	14.9	0.1
5	α-CD (AA)	40	108 046	15.0	0.01
6	α-CD (CG)	40	108 060	15.0	0.8
7	*cis*-AzoC10 (CG)	500	994 712	31.1	6.4
8	*cis*-AzoC10 (CG)	1000	984 848	31.2	6.4
9	*cis*-AzoC10 (CG)	1500	974 252	31.2	6.4
10	*cis*-AzoC10 (CG)	2000	965 120	31.3	6.4 (10)
11	*trans*-AzoC10 (CG)	500	995 048	31.1	5.6
12	*trans*-AzoC10 (CG)	1000	985 112	31.2	5.6
13	*trans*-AzoC10 (CG)	1500	975 608	31.3	5.6
14	*trans*-AzoC10 (CG)	2000	965 580	31.3	5.6 (10)
15	α-CD/*cis*-AzoC10 (CG)	768	820 508	29.9	8.0 (2)
16	α-CD/*cis*-AzoC10 (CG)	384	251 322	31.5	8.0 (2)
17	α-CD/*cis*-AzoC10 (CG)	192	248 830	31.3	8.0 (2)
18	α-CD/*trans*-AzoC10 (CG)	40	144 896	16.4	8.0 (2)

[a] The number of water molecules was 4 times that of the CG beads in the systems since the MARTINI force field uses a 4 : 1 mapping for water molecules. [b] The number in the parentheses is the number of trajectories simulated.

2.2 Mapping

Based on the mapping rule of the MARTINI force field,[37] we constructed a CG model for *cis*-, *trans*-AzoC10 and α-CD, respectively. There are four main types of beads: polar (P), nonpolar (N), apolar (C) and charged (Q) to represent the chemical nature of the underlying atomistic structures. The bead types of ring atoms are labeled by a prefix "S". Both *cis*-AzoC10 and *trans*-AzoC10 were represented by 14 CG beads (Fig. 1a). The phenyl rings in the azobenzene moiety and the oxygen atom bonded to it were represented by two equilateral triangular rings, made up of CG particles of type SC4. The double-bonded two nitrogen atoms (N=N) were represented by one bead of type N0. The hydrocarbon chains were divided sequentially into propyl, butyl, and propyl groups, represented by the particles of type C2, C1, and C2 respectively. The pyridinium group was mapped onto an equilateral triangular ring represented by particles of type SC3, SC3, and SQ0 respectively. The solvated bromide ion was represented by a bead of type Qa with unit negative charge. For *cis*- and *trans*-AzoC10 molecules, all CG beads were assigned a mass of 72 amu for chain structures and 45 amu for ring structures in our simulations.

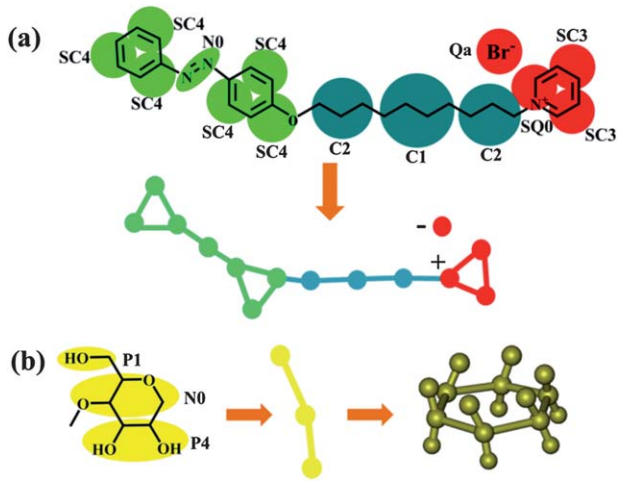

Fig. 1 Mapping from atomistic structures to CG beads for *trans*-AzoC10 and α-CD. The types of beads are labeled with the prefix "S" denoting the ring beads. The final CG models are represented by the ball-and-stick scheme. The azobenzene moiety is colored green, the alkyl chain cyan, and the hydrophilic head red. The same coloring code is used for all the figures presented in this work. The mapping and types of beads for *cis*-AzoC10 is the same as for *trans*-AzoC10.

α-CD was represented by 18 CG beads, with three beads per sugar unit (Fig. 1b). Due to the hydrophobic cavity and hydrophilic exterior nature, α-CD formed a host–guest inclusion complex with the hydrophobic azobenzene moiety of AzoC10 in aqueous solution.[19] For each glucose unit: $-CH_2OH$ of the primary rim was grouped into one bead of type P1, two –CHOH of the secondary rim were grouped into one bead of type P4, and the remaining atoms of the middle part were represented by one bead of type N0. Besides, all beads of α-CD were assigned realistic masses so that accurate kinetics can be obtained.[37]

2.3 CG force field

The force field parameters for the nonbonded interactions between CG sites were the same as the MARTINI force field,[37] and the dielectric screening factor in the current version of MARTINI is 15. The parameters for the bonded interactions in our system were very different from the standard MARTINI force field. Due to the high energy barriers,[46,47] *cis–trans* isomerization of the azobenzene moiety is not possible in the absence of visible or UV light excitation. Since we were interested in the assembly and disassembly when AzoC10 was in either *cis* or *trans* form, we can distinguish the azobenzene conformation in the CG model by applying a harmonic potential function $V_{\mathrm{angle}}(\theta) = \frac{1}{2}K_{\mathrm{angle}}(\theta - \theta_0)^2$ on the angle defined by SC4, N0, and SC4 beads with K_{angle} 10 and 30 kJ mol^{-1} rad^{-2}, θ_0 120° and 180°, for *cis*- and *trans*-azobenzene, respectively. To model the host–guest interactions between α-CD and AzoC10, the cavity of α-CD should be kept rigid. So all the bond length terms were replaced by an appropriate set of constraints, and the force constants assigned for angles were larger than the original MARTINI force field; furthermore, the proper dihedral potential $V_{\mathrm{pd}}(\phi) = K_{\mathrm{pd}}[1 + \cos(\phi - \phi_{\mathrm{pd}})]$ with a multiplicity of 1 and the improper dihedral angle potential $V_{\mathrm{id}}(\phi) = K_{\mathrm{id}}(\phi - \phi_{\mathrm{id}})^2$ were applied. As for the solvent water molecules, we adopted a standard MARTINI CG model[37] directly. Because of the smoother potential functions of the CG model compared to the AA model, the dynamics of CG simulation is significantly faster. On the basis of a comparison of diffusion rates of real water and CG water, and the dynamics of alkanes and lipids, a scaling factor of 4 was used for the timescale interpretation.[37] The timescale used to present the results below is effective, *i.e.*, the simulation time multiplied by a factor of 4.

All the simulations were performed with the GROMACS package (version 4.5.4)[48] in an *NPT* ensemble with $T = 300$ K and $P = 1$ atm. The weak couplings to external heat and pressure baths were applied based on the Berendsen scheme.[49] Before starting MD simulations, an energy minimization using the steepest descent algorithm was performed. Periodic boundary conditions were applied in all directions to minimize the edge effects in a finite system. Trajectory analysis were done with the help of utility tools included in the GROMACS[48] and VMD[45] packages.

3 Results and discussion

3.1 Micellar structure comparison: AA *vs.* CG molecular dynamics simulations

The application of the MARTINI force field to our system is straightforward, though we have to make necessary modifications to address our question, the photo-controlled assembly, as mentioned above. In general, the MARTINI force field is transferrable, but before applying it to a new system and addressing a specific question, we have to validate it. In case the amphiphilicity is essential, it is a standard practice to compare the micellar structure between AA and CG models. The snapshots of both *cis*- and *trans*-AzoC10 micellar structures, as well as the radial distribution function (RDF) profiles for each chemical group of the surfactants as a function of the center-of-mass (COM) distance between that group and the entire micelle, are shown in Fig. 2 for AA and CG models. It is clear that, for either of the surfactants, the final equilibrated micelle structures generated from the equilibrium simulations of 10 ns and 200 ns with AA and CG models, respectively, are quite similar. The RDFs were generated using the trajectories towards the end of the simulation when the micelles were in relatively stable conformations. The peaks of the RDFs coincide with each other within 0.15 nm, for each chemical group of the surfactants. The water molecules penetrate into the micelle to a somewhat larger extent in the AA simulations, which is simply caused by representing four realistic water molecules with one single CG solvent particle in the CG simulations. Moreover, it is apparent that the peak positions of RDFs of each component such as the azobenzene moieties, the alkyl chains, and the charged head groups appear in an order of increased distance to the micellar center. So, a common feature of the micelles in our simulations is that the azobenzene groups are packed tightly, while the carbon chains and the charged head groups are packed loosely. A comparison between AA and CG models for α-CD is provided in the ESI.†

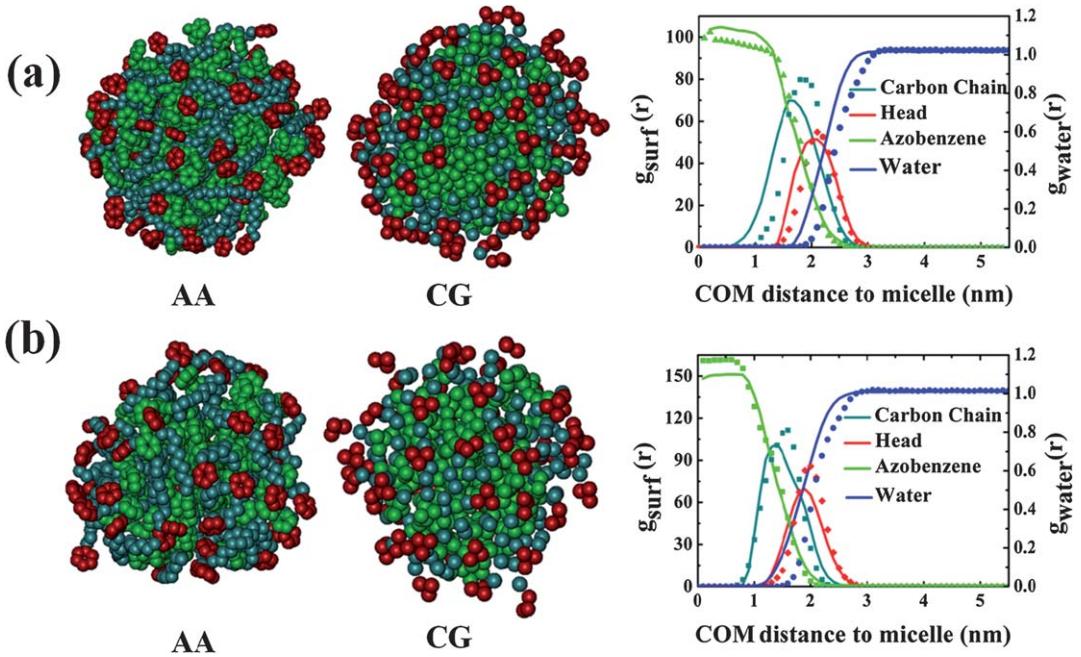

Fig. 2 Snapshots of the equilibrated micelle structures and RDFs from the center-of-mass (COM) of each surfactant group to that of the micelle for (a) *cis*-AzoC10 and (b) *trans*-AzoC10 compared between AA (solid lines) and CG (symbols) models. The azobenzene moiety is colored green, the alkyl chain cyan, and the hydrophilic head red. The hydrogen atoms in the AA model and the water molecules in both models are not shown for clarity.

3.2 Aggregation of *cis*-AzoC10 and *trans*-AzoC10

Fig. 3 shows snapshots taken during the aggregation of $N = 500$ *cis*-AzoC10 (upper panel), $N = 2000$ *cis*-AzoC10 (middle panel), and $N = 2000$ *trans*-AzoC10 (lower panel). For $N = 500$ *cis*-AzoC10 starting from a random distribution in aqueous solution, surfactant monomers first aggregate into small clusters, and then these small clusters coalesce to form spherical micelles. At the final stage of aggregation, the majorities of the aggregates are spherical micelles. A similar behavior was observed for $N = 500$ *trans*-AzoC10. For *cis*-AzoC10 and *trans*-AzoC10 with $N = 2000$ monomers starting from random distributions, we observed a rapid local aggregation into small clusters, which coalesce to larger clusters or spherical micelles. The larger clusters or spherical micelles further coalesce into disk-like micelles in the case of *cis*-AzoC10 and worm-like micelles in the case of *trans*-AzoC10. It is noted that micelles of different shapes and sizes co-exist in aqueous solution at high surfactant concentrations. Ten simulations were performed for either *cis*- or *trans*-AzoC10, starting from random distributions of $N = 2000$ monomers in the simulation box. At the final stage of simulations, the size distribution of the aggregates was counted and is presented in Fig. 4. It shows that for *cis*-AzoC10 about 0.48 of the micelles are disk-shaped, and for *trans*-AzoC10 about 0.52 are worm-like. For both *cis*- and *trans*-AzoC10, when the number of monomers in the aggregates is below 100, the micelles are spherical, and when the size of aggregates is above 100, the micelles turn into disk-like in the case of *cis*-AzoC10 and worm-like in the case of *trans*-AzoC10. The different shapes of aggregates can be attributed to different molecular structures of monomers. The compact *cis* form of azobenzene is more bulky than the extended *trans* form. The packing of *cis*-AzoC10 is not easy to regulate to form irregular worm-like micelles as *trans*-AzoC10 does. As a result, *cis*-AzoC10 tends to form disk-like micelles, which are more ordered than worm-like micelles. Our simulation results clearly showed that the shape of aggregates has a strong dependence on the molecular structure and concentrations of monomers. The predictions made on the size distributions of micelles are anticipated to be tested by solution scattering experiments in the future.

The clustering analyses have been performed, by the modified *g_clustsize* program of Wu,[50] to gain more information on the aggregation dynamics. When any of the tail particles in two surfactants are separated by no more than a cutoff distance of 0.5 nm, they are regarded as belonging to the same cluster. By our definition, a cluster is constituted by at least two monomers. If none of the monomers satisfies the above condition, the number of clusters is zero. Fig. 5 plots the time evolution of the number of monomers that do not belong to any cluster, the number of clusters and the average size of clusters for *cis*-AzoC10 during the aggregation process with a total number of surfactants $N = 500$, 1000, 1500 and 2000, respectively. Similar analysis for *trans*-AzoC10 is provided in Fig. S2 of the ESI.† It can be seen that the number of clusters suddenly increases and reaches a maximum within tens of nanoseconds, which corresponds to the first stage of aggregation, the nucleation. Meanwhile, the number of isolated monomers decreases quickly. The average size of clusters, defined as the average number of monomers in clusters, was plotted as a function of simulation time on a log–log scale to show the dynamics properly. The first stage, $t < 0.03$ μs, is the nucleation of spherical micelles. The second stage, 0.03 μs < t

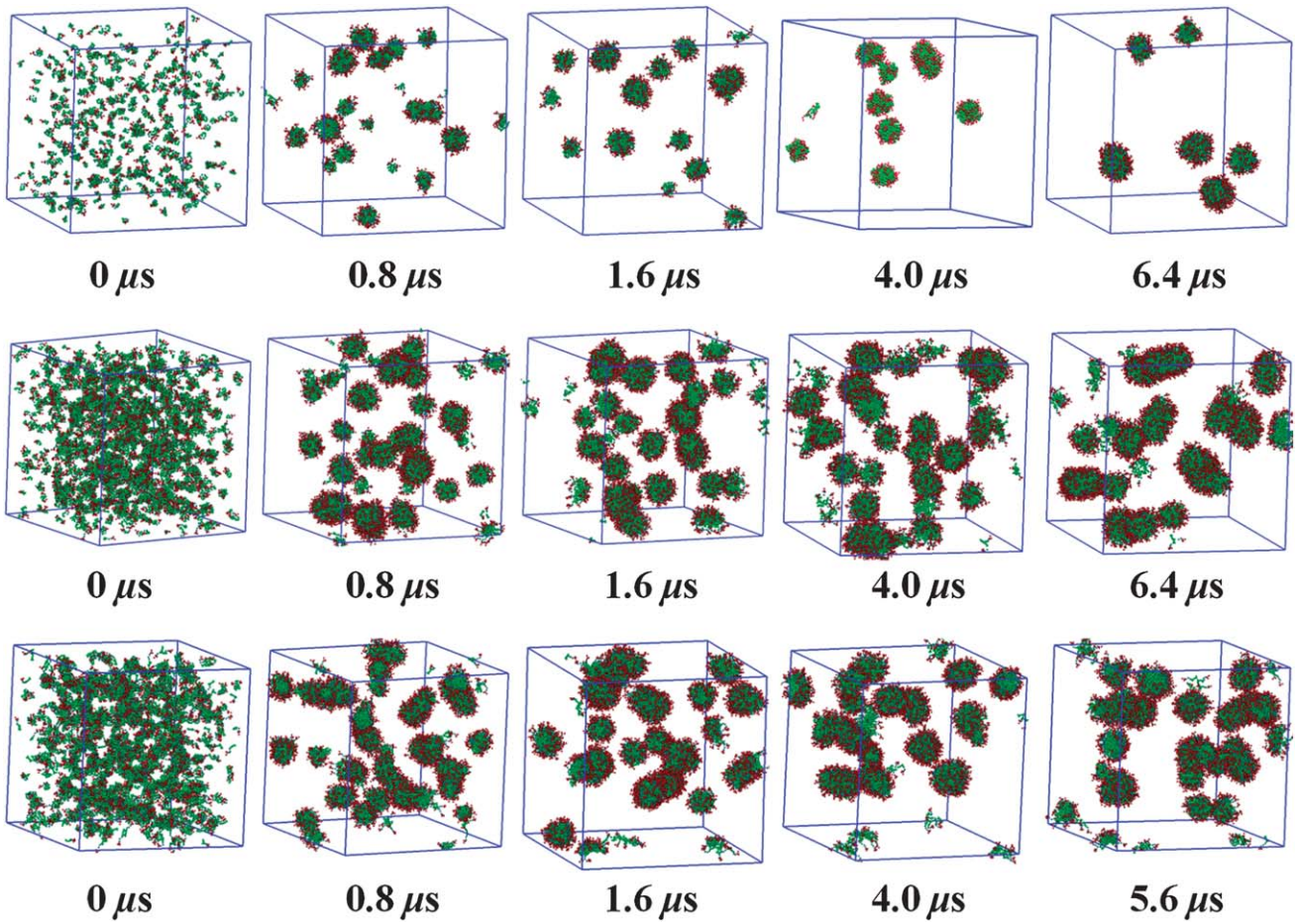

Fig. 3 Snapshots taken in the simulation of 500 *cis*-AzoC10 (upper), 2000 *cis*-AzoC10 (middle) and 2000 *trans*-AzoC10 (lower) aggregating into micelles. The CG water particles are not shown for clarity.

< 0.3 μs, is the formation and growth of spherical micelles. The aggregation dynamics at this stage obeys a power law of $t^{0.5}$, which is consistent with the Smoluchowski theory of diffusion-limited aggregation.[51] After that, an increase in the cluster size *via* cluster fusion is significantly slowed down due to repulsive interactions between the charged head groups. This stage corresponds to the formation of the disk-like or worm-like micelles.

3.3 Self-assembly of α-CD/*cis*-AzoC10 complexes

In the following, the impact of α-CD on the assembly is discussed. Our previous all-atom simulations[19] showed that *cis*-AzoC10/α-CD is amphiphilic with the long alkyl chain of *cis*-AzoC10 encapsulated in the cavity of α-CD and the nonpolar *cis*-azobenzene moiety exposed to the bulk water. To investigate the assembly of *cis*-AzoC10/α-CD, we performed CG simulations starting from an ordered arrangement of the complexes on a three-dimensional lattice, solvated in a cubic box of water with a side length of 30 nm. The duration of the simulation was over 8.0 μs. Fig. 6 contains snapshots illustrating the aggregation process of *cis*-AzoC10/α-CD with N = 192, 384, and 768 inclusion complexes in the box. Starting from an ordered arrangement, we first observed a rapid local clustering, which then merges into inter-connected worm-like structures. Next, these irregular structures transform themselves into large single worm-like micelles. Most α-CDs have shuttled to the pyridinium side of *cis*-AzoC10 with the azobenzene moiety completely excluded from the cavity. The hydrophobic azobenzene moieties aggregate to form the inner core of worm-like micelles, and the hydrophilic pyridinium head groups are located at the outermost of worm-like micelles (see Fig. S4†). The hydrophobic carbon chains, included in the cavity of α-CD, are either extended or bent to regulate the position of α-CDs. α-CDs surround the surface of worm-like micelles and protect the hydrophobic azobenzene moiety from being exposed to water. However, due to the bulky size of α-CD, some hydrophobic azobenzene groups are still exposed and loosely packed. Due to the special property of α-CD, the amphiphilicity of *cis*-AzoC10/α-CD is relatively weak, and the assembly was slower than that of either *cis*- or *trans*-AzoC10. In contrast to *cis*- or *trans*-AzoC10, *cis*-AzoC10/α-CD aggregates into worm-like micelles at all concentrations, and the micelles are not spherical irrespective of their size. Moreover, the size and shape of micelles formed by *cis*-AzoC10/α-CD are different from those formed by pure AzoC10.

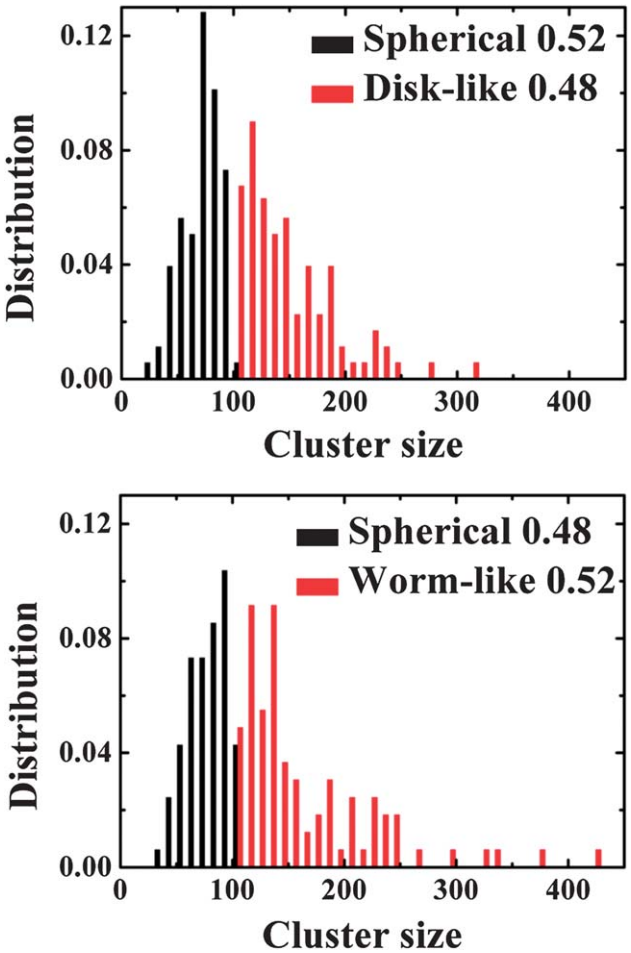

Fig. 4 Size distribution of the micelles at the final stage of simulations with $N =$ 2000 monomers: *cis*-AzoC10 (top) and *trans*-AzoC10 (bottom). Ten trajectories were used to obtain the distribution for either *cis*- or *trans*-AzoC10. The shape of the micelles was also denoted.

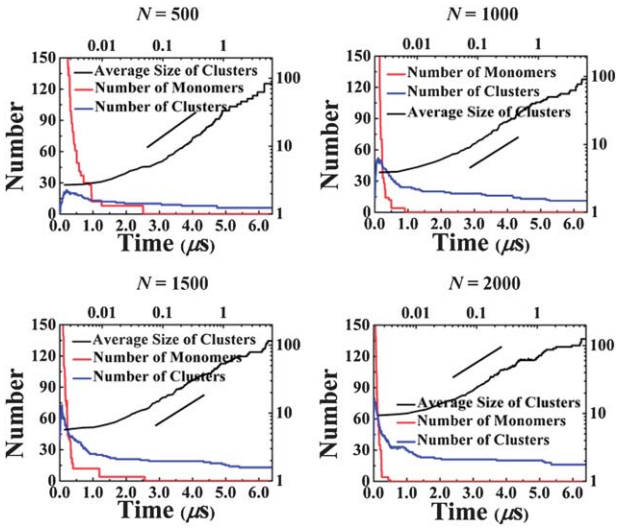

Fig. 5 Time evolution of the number of monomers, the number of clusters, and the average size of clusters in the aggregation of *cis*-AzoC10 with $N =$ 500, 1000, 1500, and 2000, respectively.

3.4 Disassembly of *trans*-AzoC10/α-CD

In *trans*-AzoC10/α-CD, the hydrophobic azobenzene moiety is included axially in the cavity of α-CD,[19] so *trans*-AzoC10/α-CD is no longer amphiphilic. Finally, to mimic the disassembly experiments of *trans*-AzoC10/α-CD in aqueous solution, we set up a pre-assembled micelle of $N = 40$ monomers (Fig. 7a) with the help of PACKMOL program.[44] For each inclusion complex, the azobenzene moiety is included in the central cavity of α-CD; thus, in this pre-assembled starting configuration, the bulky α-CDs are located at the inner core of the micelle. And then, the pre-assembled structure was solvated in a cubic box filled with roughly 36 224 pre-equilibrated CG water. Next, we minimized the energy of the solvated system and confirmed the absence of CG water particles in the inner core of the micelle. After the above preparation, we performed CG molecular dynamics simulations of 8.0 μs. Fig. 7b shows the final configuration of *trans*-AzoC10/α-CD in aqueous solution at the end of simulation. It is clear that: (1) most α-CDs are dispersed into the bulk water and CG water particles have penetrated into the micelle; thus, *trans*-AzoC10/α-CD are separated from each other and surrounded by water; (2) the azobenzene moiety is still included in the α-CD cavity of each *trans*-AzoC10/α-CD inclusion complex; (3) although *trans*-AzoC10/α-CD are isolated, they are close to each other in space, and there are local aggregations of α-CDs in a shoulder by shoulder manner.

Fig. 7c plots the atomistic water distributions within 5 Å of each chemical group: azobenzene, carbon chain, pyridinium head and α-CD at the beginning, final, and completely "disassembled" stage of *trans*-AzoC10/α-CD disassembly. At $t = 0$ μs, the *trans*-azobenzene moiety encapsulated in α-CD is packed in the inner core of the micelle, due to the bulky size of α-CD, the packing is quite loose. After solvation, there are about 2 to 3 water molecules on average in the vicinity of azobenzene, and 8 water molecules in the vicinity of α-CD. The hydrophobic carbon chains extend freely in the outer shell of the micelle, and the number of water molecules within 5 Å is about 5. As for the outermost packed head groups, the solvation is complete, and the number of water molecules within 5 Å is about 11. At $t =$ 8.0 μs, α-CDs with azobenzene included are dispersed into the bulk, so water molecules have increased significantly to 21, and correspondingly the number of water molecules within 5 Å of azobenzene have increased to 5. Because carbon chains are bent after 8 μs simulation, the number of water molecules decreased to 4. At the final stage of simulation, though disassembled *trans*-AzoC10/α-CD are still confined in space, leading to water distribution around the head group less than that at the beginning of simulation.

To better illustrate the degree of disassembly, we performed a contrast simulation. The starting configuration for this simulation was generated by randomly placing 40 *trans*-AzoC10/α-CD in a cubic box and solvated. A 100 ns CG simulation was performed. Water distribution in the neighborhood of each residue was calculated using the trajectory near the end of the simulation. The statistical result was plotted and labeled as "disassembled" in Fig. 7c. It represents water distribution of

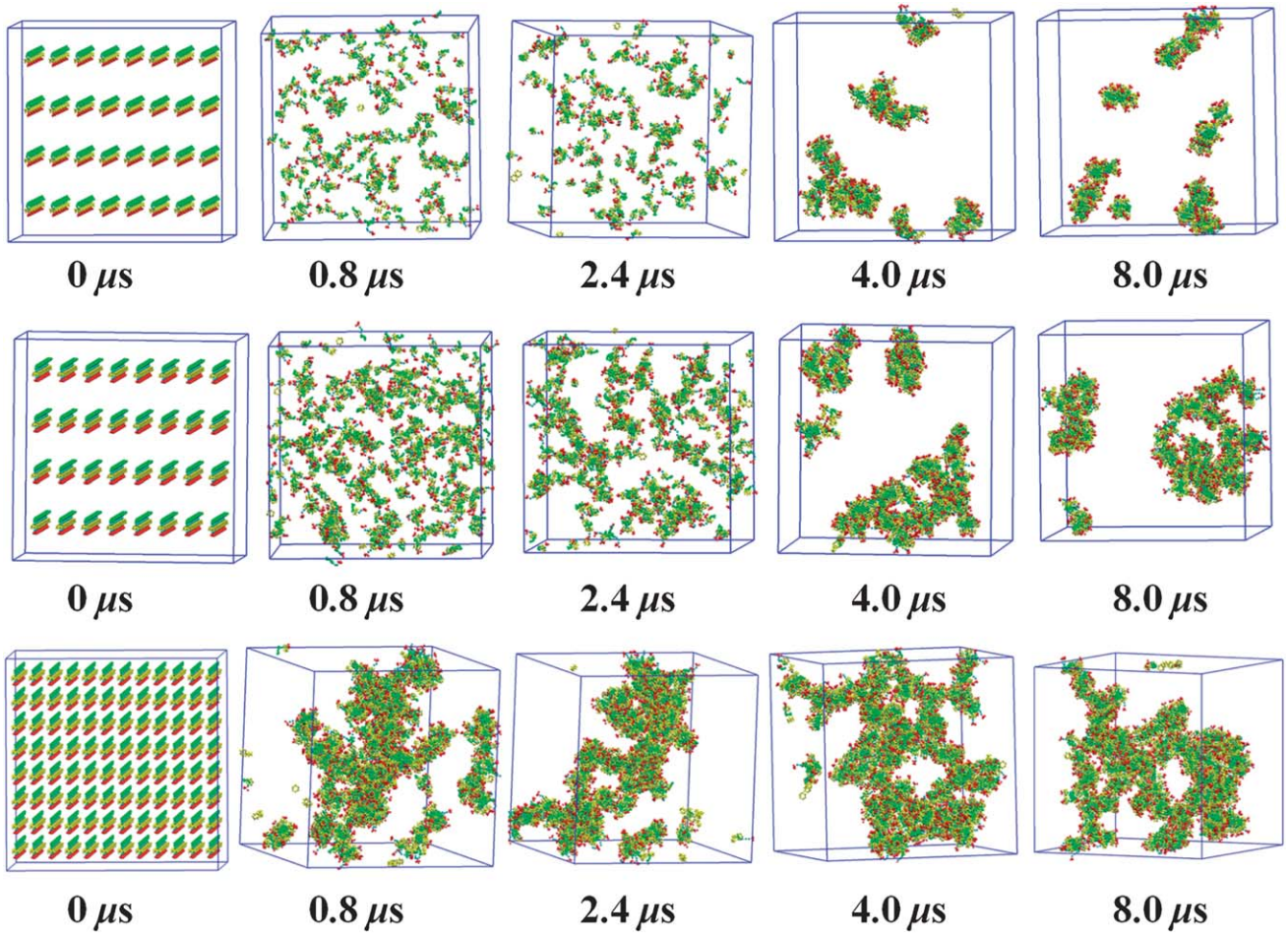

Fig. 6 Snapshots taken in the aggregation of the *cis*-AzoC10/α-CD inclusion complexes, with $N = 192$, 384, and 768 respectively. The CG water particles are not shown for clarity.

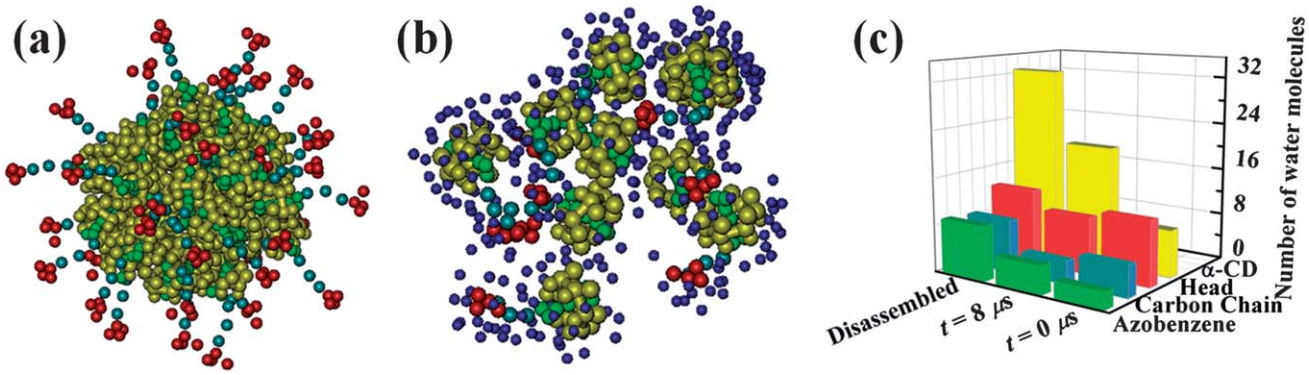

Fig. 7 (a) The micelle structure at the beginning of the disassembly simulation built with *trans*-AzoC10/α-CD. The CG water particles are not shown for clarity. (b) The final structures at the end of 8 μs simulation. The blue beads represent CG water particles. (c) The atomistic water distributions within 5 Å of each residue: azobenzene (green), carbon chain (cyan), head group (red) and α-CD (yellow) at the beginning ($t = 0$ μs) and end ($t = 8.0$ μs) of the simulation, as well as in the completely disassembled state which was obtained by equilibrating randomly distributed *trans*-AzoC10/α-CD in a box of water.

trans-AzoC10/α-CD in a completely disassembled state. It is clear that water distribution around all residues in the "disassembled" state is larger than that observed in the final configuration of the disassembly simulation at $t = 8$ μs. So, though disassembled at the end of the simulation starting from a pre-assembled micelle, *trans*-AzoC10/α-CD are still confined in space and it will take much more time for them to fill the entire box.

4 Conclusions

The CG model offers several orders of magnitude speedup in molecular dynamics simulations as compared to those based on atomistic descriptions. In this work, we used CG molecular dynamics simulations and the modified MARTINI force field to investigate aggregation of *cis*-, *trans*-AzoC10, and *cis*-AzoC10/α-CD into micelles in aqueous solution. The size and shape of spontaneously assembled micelles with *cis*-AzoC10, *trans*-AzoC10, and the *cis*-AzoC10/α-CD were analyzed. The simulations of *cis*- and *trans*-AzoC10 at different concentrations on a timescale of ten microseconds have revealed a significant shape dependence of aggregates on the molecular structure and concentrations of monomers. At low concentrations, both *cis*- and *trans*-AzoC10 aggregated exclusively into spherical micelles. At high concentrations, disk-like and spherical micelles co-existed in the case of *cis*-AzoC10, and worm-like and spherical micelles co-existed in the case of *trans*-AzoC10. The aggregation dynamics within the simulation time can be divided into three stages: the rapid nucleation at $t < 0.03$ μs; the formation and growth of spherical micelles at 0.03 μs $< t <$ 0.3 μs; and finally, the formation of disk-like or worm-like micelles at $t > 1$ μs. Due to the loss of amphiphilicity, disassembly of a pre-assembled micelle with *trans*-AzoC10/α-CD was observed. In conclusion, to study the photo-controlled assembly, CG models have to be carefully designed in order to capture the amphiphilicity change caused by host–guest interactions and photo-isomerization. CG molecular dynamics simulations are anticipated to be a useful tool in the study of controlled assembly and disassembly to bridge the gap between atomistic simulations and experiments.

Acknowledgements

We are indebted to Professor Siewert-Jan Marrink for helpful discussions about the usage of the MARTINI force field, and his student Cesar Lopez Bautista for kindly helping us build the coarse-grained model for α-cyclodextrin. We thank Dr Rongliang Wu for kindly providing us the modified g_clustsize program for trajectory analysis. This work is supported by the National Natural Science Foundation of China (20903060) and the Innovative Research Groups of the National Natural Science Foundation of China (21121004).

Notes and references

1 B. L. Feringa, R. A. van Delden, N. Koumura and E. M. Geertsema, *Chem. Rev.*, 2000, **100**, 1789.
2 V. Balzani, A. Credi, F. M. Raymo and J. F. Stoddart, *Angew. Chem., Int. Ed.*, 2000, **39**, 3348.
3 Q. Jin, G. Liu, X. Liu and J. Ji, *Soft Matter*, 2010, **6**, 5589.
4 Y. Wang, N. Ma, Z. Wang and X. Zhang, *Angew. Chem., Int. Ed.*, 2007, **46**, 2823.
5 Y. Wang, P. Han, H. Xu, Z. Wang, X. Zhang and A. V. Kabanov, *Langmuir*, 2010, **26**, 709.
6 K. Han, W. Su, M. Zhong, Q. Yan, Y. Luo, Q. Zhang and Y. Li, *Macromol. Rapid Commun.*, 2008, **29**, 1866.
7 T. Ikeda and O. Tsutsumi, *Science*, 1995, **268**, 1873.
8 N. Tamai and H. Miyasaka, *Chem. Rev.*, 2000, **100**, 1875.
9 G. S. Hartley, *Nature*, 1937, **140**, 281.
10 J. Henzl, M. Mehlhorn, H. Gawronski, K.-H. Rieder and K. Morgenstern, *Angew. Chem., Int. Ed.*, 2006, **45**, 603.
11 T. Hugel, N. B. Holland, A. Cattani, L. Moroder, M. Seitz and H. E. Gaub, *Science*, 2002, **296**, 1103.
12 T. Schultz, J. Quenneville, B. Levine, A. Toniolo, T. J. Martínez, S. Lochbrunner, M. Schmitt, J. P. Shaffer, M. Z. Zgierski and A. Stolow, *J. Am. Chem. Soc.*, 2003, **125**, 8098.
13 I. Willner, *Acc. Chem. Res.*, 1997, **30**, 347.
14 R. Behrendt, C. Renner, M. Schenk, F. Wang, J. Wachtveitl, D. Oesterhelt and L. Moroder, *Angew. Chem., Int. Ed.*, 1999, **38**, 2771.
15 L. Guerrero, O. S. Smart, C. J. Weston, D. C. Burns, G. A. Woolley and R. K. Allemann, *Angew. Chem., Int. Ed.*, 2005, **44**, 7778.
16 G. Bottari, D. A. Leigh and E. M. Pérez, *J. Am. Chem. Soc.*, 2003, **125**, 13360.
17 D. Qu, Q. Wang, X. Ma and H. Tian, *Chem.–Eur. J.*, 2005, **11**, 5929.
18 C. A. Stanier, M. J. O'Connell, W. Clegg and H. L. Anderson, *Chem. Commun.*, 2001, 493.
19 X. Zheng, D. Wang, Z. Shuai and X. Zhang, *J. Phys. Chem. B*, 2012, **116**, 823.
20 M. L. Klein and W. Shinoda, *Science*, 2008, **321**, 798.
21 G. A. Voth, *Coarse-Graining of Condensed Phase and Biomolecular Systems*, CRC Press, Boca Raton, FL, 2009.
22 S. Tamesue, Y. Takashima, H. Yamaguchi, S. Shinkai and A. Harada, *Angew. Chem., Int. Ed.*, 2010, **49**, 7461.
23 B. J. Ravoo and R. Darcy, *Angew. Chem., Int. Ed.*, 2000, **39**, 4324.
24 K. Liu, C. Wang, Z. Li and X. Zhang, *Angew. Chem., Int. Ed.*, 2011, **50**, 4952.
25 A. P. Lyubartsev and A. Laaksonen, *Phys. Rev. E*, 1995, **52**, 3730.
26 A. P. Lyubartsev and A. Laaksonen, *Phys. Rev. E*, 1997, **55**, 5689.
27 A. P. Lyubartsev and A. Laaksonen, *J. Chem. Phys.*, 1999, **111**, 11207.
28 J. C. Shelley, M. Y. Shelley, R. C. Reeder, S. Bandyopadhyay and M. L. Klein, *J. Phys. Chem. B*, 2001, **105**, 4464.
29 J. C. Shelley, M. Y. Shelley, R. C. Reeder, S. Bandyopadhyay, P. B. Moore and M. L. Klein, *J. Phys. Chem. B*, 2001, **105**, 9785.
30 S. Izvekov, M. Parrinello, C. J. Burnham and G. A. Voth, *J. Chem. Phys.*, 2004, **120**, 10896.
31 S. Izvekov and G. A. Voth, *J. Chem. Phys.*, 2005, **123**, 134105.
32 S. Izvekov and G. A. Voth, *J. Phys. Chem. B*, 2005, **109**, 2469.
33 S. Izvekov and G. A. Voth, *J. Chem. Theory Comput.*, 2006, **2**, 637.
34 S. Izvekov and G. A. Voth, *J. Chem. Phys.*, 2006, **125**, 151101.
35 L. Lu and G. A. Voth, in *Advances in Chemical Physics*, ed. S. A. Rice and A. R. Dinner, John Wiley & Sons, Inc., Hoboken, 2012, vol. 149, p. 47.
36 S. J. Marrink, A. H. de Vries and A. E. Mark, *J. Phys. Chem. B*, 2004, **108**, 750.
37 S. J. Marrink, H. J. Risselada, S. Yefimov, D. P. Tieleman and A. H. de Vries, *J. Phys. Chem. B*, 2007, **111**, 7812.

38 M. Orsi, D. Y. Haubertin, W. E. Sanderson and J. W. Essex, *J. Phys. Chem. B*, 2008, **112**, 802.
39 B. Smit, P. A. J. Hilbers, K. Esselink, L. A. M. Rupert, N. M. Vanos and A. G. Schlijper, *Nature*, 1990, **348**, 624.
40 C. A. López, A. J. Rzepiela, A. H. de Vries, L. Dijkhuizen, P. H. Hünenberger and S. J. Marrink, *J. Chem. Theory Comput.*, 2009, **5**, 3195.
41 J.-B. Maillet, V. Lachet and P. V. Covney, *Phys. Chem. Chem. Phys.*, 1999, **1**, 5277.
42 S. K. Samanta, S. Bhattacharya and P. K. Maiti, *J. Phys. Chem. B*, 2009, **113**, 13545.
43 P. K. Maiti, Y. Lansac, M. A. Glaser and N. A. Clark, *Langmuir*, 2002, **18**, 1908.
44 L. Martínez, R. Andrade, E. G. Birgin and J. M. Martínez, *J. Comput. Chem.*, 2009, **30**, 2157.
45 W. Humphrey, A. Dalke and K. Schulten, *J. Mol. Graphics*, 1996, **14**, 33.
46 E. Wei-Guang Diau, *J. Phys. Chem. A*, 2004, **108**, 950.
47 M. L. Tiago, S. Ismail-Beigi and S. G. Louie, *J. Chem. Phys.*, 2005, **122**, 094311.
48 D. Van de Spoel, E. Lindahl, B. Hess, A. R. Buuren, E. Apol, P. J. Meulenhoff, D. P. Tieleman, A. L. Sijbers, K. A. Feenstra, R. Drunen and H. J. Berendsen, *Gromacs User Manual version 4.5*, 2010.
49 H. J. C. Berendsen, J. P. M. Postma, W. F. van Gunsteren, A. DiNola and J. R. Haak, *J. Chem. Phys.*, 1984, **81**, 3684.
50 R. Wu, M. Deng, B. Kong and X. Yang, *J. Phys. Chem. B*, 2009, **113**, 15010.
51 N. Arai, K. Yasuoka and Y. Masubuchi, *J. Chem. Phys.*, 2007, **126**, 244905.